Plastic flow in shock-loaded silver at strain rates from 10^4 s^{-1} to 10^7 s^{-1} and temperatures from 296 K to 1233 K

E. B. Zaretsky[1,a)] and G. I. Kanel[2]
[1]*Department of Mechanical Engineering, Ben Gurion University, 84105 Beer Sheva, Israel*
[2]*Joint Institute for High Temperatures RAS, Izhorskaya 13, bld. 2, 125412 Moscow, Russia*

(Received 17 July 2011; accepted 22 August 2011; published online 3 October 2011)

The evolution of elastic-plastic shock waves in 99.9% purity silver samples of 0.127 to 2.0 mm thickness has been studied in a series of VISAR-instrumented planar impact experiments with initial sample temperature varied from 296 to 1233 K. The decay of elastic precursor wave at 933, 1173, and 1233 K temperatures is approximately inversely proportional to the square root of the propagation distance. The latter corresponds to the cubic dependence of initial plastic strain rate, ranged from 10^4 s^{-1} to 10^6 s^{-1}, on the shear stress. At fixed strain rates, the flow stress grows linearly with the temperature but the dependence becomes stronger near the silver melting point, 1234 K. An analysis of the rise times of the plastic shock waves shows that for the same level of shear stress the plastic strain rate at the shock front is significantly higher than that at the top of the elastic precursor wave. © *2011 American Institute of Physics*. [doi:10.1063/1.3642989]

I. INTRODUCTION

The dependences of the yield stress and of the tensile strength on the strain rate and temperature at high strain rates provide information regarding the basic mechanisms of plastic deformation and fracture. The flow stress of crystalline solids is known to increase with the strain rate. For many metals this tendency is strengthened sharply when the rate of deformation exceeds 10^3–10^4 s^{-1}.[1,2] This strengthening is attributed to the transition in the mode of dislocation motion. For low loading rates, the dislocation motion is supported by thermal fluctuations; the mutual action of the applied stress and of the thermal activation helps dislocations to overcome the obstacles.[1] Increasing thermal fluctuations facilitate not only the motion of dislocations but also their homogeneous nucleation;[3] at low strain rates the increasing temperature results in a decline of the yield stress. At high strain rate loading, 10^3 s^{-1} and above, the applied stress is high enough for dislocation crossing the obstacles with no aid of thermal fluctuations. Under these conditions, a viscous phonon drag may become the dominant resistance of the lattice to the motion of dislocations. Since the phonon drag is proportional to the temperature[4] at the highest strain rates an increase of the flow stress with temperature may be expected. Atomistic simulations of the dislocation motion show that the dislocation velocity decreases with temperature and that the responsibility for this deceleration is due to thermal phonons.[5] The same factors, namely, the temperature and the strain rate, should, through the processes of nucleation and growth of voids, affect the tensile strength of solids.

Recent studies[6–13] of the impact response of both the polycrystalline and single crystal metals have revealed their unusual behavior at elevated temperatures. In some cases the dynamic yield stress may increase with temperature or stay unchanged while in other cases the dynamic yield stress decreases with heating. The resistance of the metals to the high-rate tensile fracture was found virtually independent of heating to, at least, 0.85 of the absolute melting temperature T_m. At temperature higher than 0.85 T_m the behavior of the tensile strength depends on the material structure. Whereas polycrystalline metals exhibit a precipitous decrease of the strength to practically zero as soon as the temperature approaches T_m, the dynamic tensile strength of single crystals remains high even close to T_m. The latter is in a reasonable agreement with the results of molecular dynamics simulations of spall fracture in copper[14] which confirm the existence of substantial spall strength of the metal beyond the melting.

In spite of these observations, information about the rate and temperature dependence of the high strain rate yield and tensile strength of metals is still scarce and insufficient for constructing general constitutive models and relationships. The lack of such information provided a motivation for the present study. Face centered cubic silver was chosen as a typical metal with multiple glide systems and low, about 20 mJ/m^2,[15] stacking fault energy displaying a relatively low shear strength. An important factor for this choice was the availability of complete set of silver elastic constants, C_{11}, C_{12}, and C_{44}, over a temperature interval from 300 to 1173 K.[16] From the single crystal data it is possible to derive the sound velocities in the polycrystalline aggregates,[17] necessary for analysis of experimental data.

The present study was based on the measurement and analysis of the shock compression waves generated in the silver samples by planar impact. The initial temperature of the samples was varied in these experiments from the ambient to 1233 K, about 2 K below the silver melting point.[18] Two approaches can be used for obtaining information about the relation between the flow stress and the rate of plastic deformation. The first one relies on the observation of the decay of the elastic precursor wave with propagation distance.[19,20] Measurements of this type were recently performed with aluminum samples of different thicknesses resulting in wave propagation distances that varied from 0.5 to 1.2 μm,[20] 40–180 μm,[22] 0.08–1 mm,[23] and 0.25–10 mm.[9] The apparent Hugoniot elastic limit (HEL) in these experiments decreased

a)Author to whom correspondence should be addressed. Electronic mail: zheka@bgu.ac.il.

by more than 2 orders of magnitude, from 12.6 GPa at submicron propagation distance to 0.05 GPa at the distance of about 10 mm. Another approach is based on the determination of the steepness of the steady plastic shock wave.[24–27] In the present study both approaches were employed in the analysis of the experimental data.

II. MATERIALS AND EXPERIMENTAL PROCEDURES

Annealed silver foils of 99.9 % purity having thickness of 0.127, 0.280, 0.5, 1.0, and 2 mm were obtained from Alfa Aesar Company. Independently of their thickness the foils contained randomly oriented globular grains of 12 μ average diameter. Square, 12 mm × 12 mm, samples of 2 and 1 mm thick were cut from the as-received foils and lapped to 0.3 mrad parallelism. The density (Archimedes method) and the speeds of sound (pulse-echo method) were measured with 2 mm samples. The initial density ρ_0 of the studied silver was found equal to 10.472 ± 0.005 kg/m^3. The longitudinal, c_l, and the shear, c_s, sound speeds were found equal to 3730 ± 20 m/s and 1740 ± 20 m/s, respectively. This yields for the bulk sound speed $c_b = \sqrt{c_l^2 - 4/3c_s^2} = 3140 \pm 30$ m/s.

Elastic-plastic shock waves were generated in the plane samples by impact of copper flyer plates of 0.5 or 1 mm thick launched by a 59 mm bore 4 m length gas gun. Details of the arrangement of shock-wave experiments at elevated temperatures have been described previously.[12] In order to maintain the samples' plane-parallelism during preheating the samples of 0.127, 0.280, and 0.5 mm thick were prepared as follows. The 12 mm × 12 mm, pieces of the silver foil were glued by low-viscosity cyanoacetate glue onto the surface of an optical flat. After controlling the upper sample surface planarity by the Puppitast dial gauge the 1.5 mm thick plane-parallel copper washer was fixed on the upper sample surface by high temperature cement (W. Haldenwanger Technische Keramik, Germany). The outer washer diameter was 11 mm. The inner washer diameter was varied from 6 mm for the 0.5 mm foil sample to 3 mm for the 0.127 mm foil sample. A 1.2 mm through hole in the washer provided direct contact of the thermocouple junction with the sample surface. After the cement setting the glue layer was removed by acetone. The further use of the composite sample was similar to the use of the whole one.[12] The impactor-sample misalignment did not exceed 1 mrad in all the experiments, either with the whole or the composite samples.

In the course of the experiments, the velocity histories of rear free surfaces of the samples were monitored by the velocity interferometer[28] with 224.0 m/s of the velocity-per-fringe constant that corresponds to approximately 1.2 ns of the time resolution. In order to ensure the focusing of the interferometer spot on the center of open sample surface area, the spot position was controlled with the aid of a microscope equipped with a magenta dichroic filter.

Four series of the tests have been performed. In each series, all the samples with different thicknesses were preheated to the same initial temperature (296, 973, 1173, and 1233 K) and were impacted by 0.5 or 1 mm thick copper flyer plates accelerated to velocities of around 250–260 m/s. In one room temperature test, the 0.127 mm thick sample was impacted by 0.5 mm Cu flyer plate through a 2 mm thick Cu baseplate separated from the sample by 0.3 mm gap. The test was to verify that no acceleration of a thin sample by projectile-propelled residual gases of the experimental chamber had taken place. Two additional tests with impactor velocity of about 320 m/s were performed with the 2 mm thick samples and initial temperature of 296 and 773 K. The parameters of the performed planar impact experiments are listed in Table I.

III. RESULTS OF MEASUREMENTS

The velocity histories recorded with the silver samples having the lowest (296 K) and the highest (1233 K) initial temperature are shown in Figs. 1(a) and 1(b) The free surface

TABLE I. Parameters of the planar impact experiments with silver samples.

TEST	Impactor/thickness, mm	Sample thickness, mm	Impact velocity, m/s
	Initial temperature 296 K		
AGA3[a]	Al, 1	1.986	105
AGA2	Cu,1	1.994	137
AGA1	Cu/1	1.939	315
AGA	Cu/1	2.004	236
AGAX	Cu/0.5	0.991	267
AGAXX	Cu/0.5	0.484	251
AGAXXX	Cu/0.5	0.267	246
AGAXXXX	Cu/0.5	0.127	242
AGAXXXX1[b]	Cu/0.5	0.127	252
	Initial temperature 973 K		
AGD	Cu/1	1.980	255
AGDX	Cu/0.5	0.986	244
AGDXX	Cu/0.5	0.492	243
AGDXXX	Cu/0.5	0.271	248
AGDXXXX	Cu/0.5	0.127	268
	Initial temperature 1233 K		
AGC	Cu/1	1.980	233
AGCX	Cu/0.5	1.012	243
AGCXX	Cu/0.5	0.482	239
AGCXXX	Cu/0.5	0.266	237
AGCXXXX	Cu/0.5	0.127	249
	Initial temperature 1173 K		
AGB1[c]	Cu/1	1.946	243
AGB[c]	Cu/1	1.954	256
AGBX	Cu/0.5	1.003	254
AGBXX	Cu/0.5	0.489	251
AGBXXX	Cu/0.5	0.267	300
AGBXXXX	Cu/0.5	0.127	252
	Initial temperature 773 K		
AGE1	Cu/1	1.999	326
AGE	Cu/1	1.987	245

[a]In this test impactor was aluminum plate of 1 mm thickness.
[b]In this test the 0.217 mm sample was shock-loaded by 0.5 mm Cu impactor through 2 mm Cu buffer.
[c]Two almost identical tests at 1173 K were performed in order to estimate possible scatter of the Hugoniot elastic limit of silver.

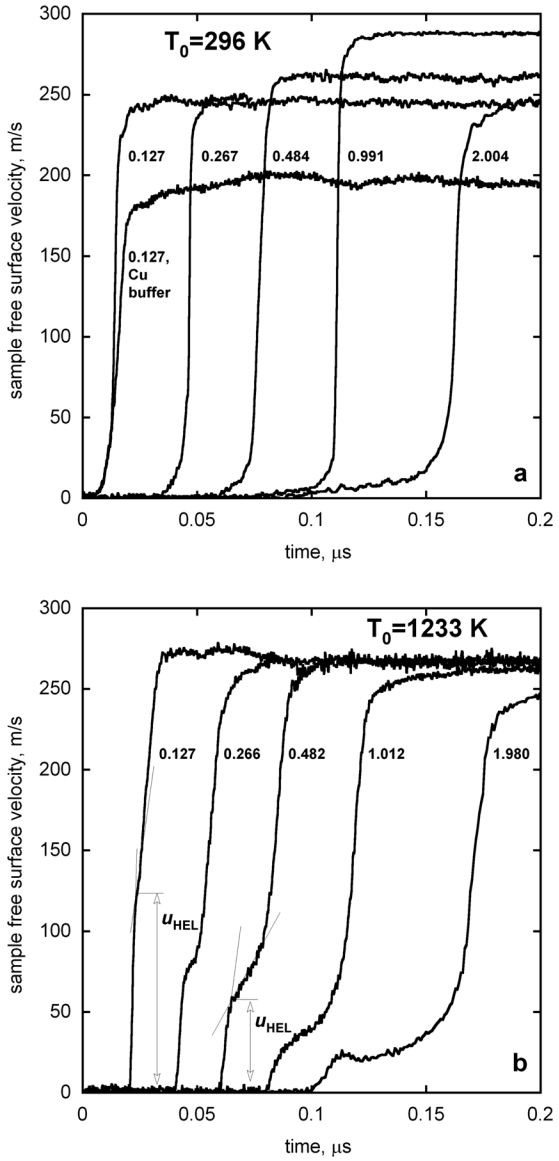

FIG. 1. Free surface velocity histories obtained with silver samples of different thickness shocked (a) at ambient temperature and (b) after preheating up to 1233 K. The sample thickness in millimeters is shown alongside the waveforms. The free surface velocities u_{HEL} corresponding to the Hugoniot elastic limit (HEL) are shown by arrows [Fig. 1(b)].

velocity history at room temperature does not show any distinct step at the front of the elastic precursor wave; the latter looks like a gradual velocity increase from an irresolvable small value. Moreover, no step-like signature is present at the velocity histories recorded at 773 K. Starting from 973 K the waveforms clearly exhibit a finite HEL whose value grows with temperature and decreases with increasing sample thickness. In the high-temperature experiments, the rise time of the elastic wave recorded with the thinnest samples is close to the temporal resolution of the VISAR. Increasing the sample thickness widens the fronts of both the elastic and plastic waves. The rise time of the plastic waves increases with heating.

A gradual increase of the Hugoniot elastic limit with heating is apparent from shown in Fig. 2 velocity histories recorded with differently preheated 2 mm thick silver samples. All the waveforms shown in Fig. 2 contain the velocity

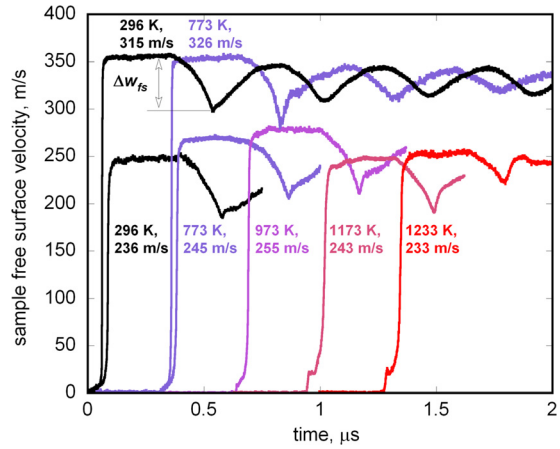

FIG. 2. (Color online) Free surface velocity histories obtained with 2 mm thick silver samples. The initial sample temperatures are shown alongside the waveforms together with the velocities of Cu impactors. The spall-related velocity pull-back is shown by arrow.

pull-back Δu_{fs} associated with the dynamic tensile (spall) strength of the material. On approaching the melting temperature, 1234 K, the pull-back value decreases substantially. Noteworthy that the HEL value measured at the closest to the melting point starting temperature, 1233 K, is the highest one.

Another important observation is that the time interval between elastic precursor wave and plastic shock wave is always larger than expected. Figure 3 presents the variation of this time interval at 1233 K as a function of the sample thickness. The departure of the experimentally measured values from those calculated on the basis of the longitudinal and shock wave speeds exceeds the effect of any reasonable dependence of the velocity of the elastic precursor wave on the stress. Moreover, the apparent velocity of the plastic wave at the distances smaller than 0.5 mm is even lower than the bulk speed of sound c_b at this temperature. Subsonic velocity

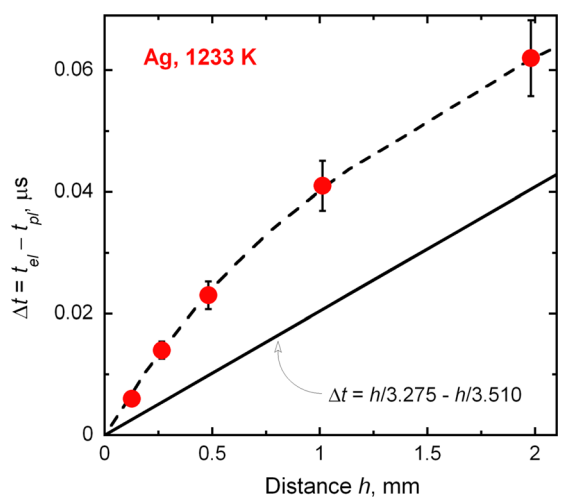

FIG. 3. (Color online) Time interval $\Delta t = t_{el} - t_{pl}$ between half-heights of the elastic precursor and the plastic wave fronts as a function of the propagation distance at 1233 K. Solid line shows the expected dependence which has been estimated for the precursor velocity equal to the longitudinal speed of sound $c_l = 3.510$ km/s at 1233 K and for the shock wave speed $U_S = 3.275$ km/s.

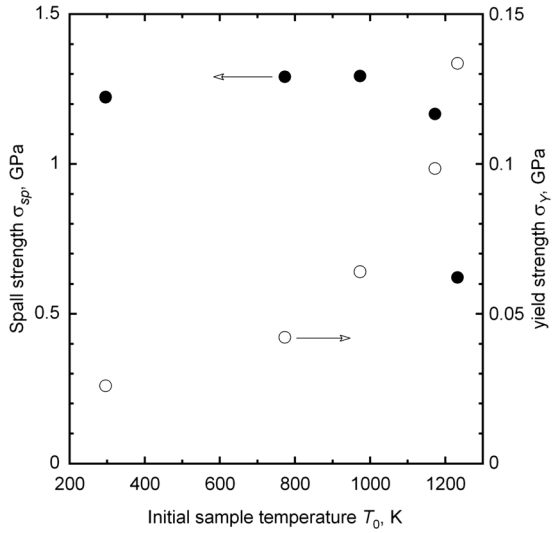

FIG. 4. Yield (open circles) and spall (filled circles) strength of silver samples of 2 mm thickness as a function of initial sample temperature T_0.

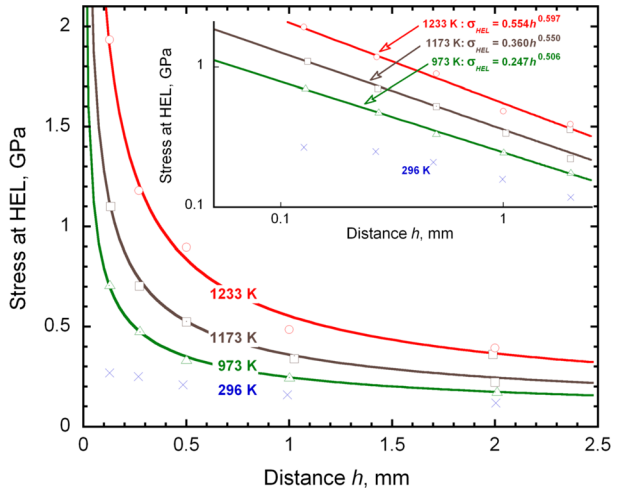

FIG. 5. (Color online) Decay of the elastic precursor wave in silver at different temperatures. The room temperature points (crosses) present estimations of the stress $\sigma_{0.05}$ corresponding to the 0.05% offset of plastic strain.

of the steady plastic shock wave is often associated with the loss of shear strength during the shock compression.[29,30] The unsteady processes in the relaxing media obviously require more sophisticated analysis which has not yet been performed.

Figure 4 presents the temperature dependences of the yield stress Y and the spall strength σ_{sp} calculated from the free surface velocity histories of 2 mm silver plates. The calculations have been done using relationships[31,32]

$$Y = \frac{3}{4}\rho_0 c_l u_{\mathrm{HEL}}\left(1 - \frac{c_b^2}{c_l^2}\right), \quad \sigma_{sp} = \frac{1}{2}\rho_0 c_b \Delta u_{fs}(1+\delta)$$

where u_{HEL} is the free surface velocity at the elastic precursor front which has been evaluated as it is shown in Fig. 1(a), Δu_{fs} is the velocity pullback, δ is the velocity correction which accounts for distortion of the waveform as a result of different propagation velocities of the spall pulse front and the rarefaction wave ahead of it. In the calculations, the temperature dependences of the density ρ_0, longitudinal sound speed c_l, and the bulk sound speed c_b were accounted for. The sound speeds for polycrystalline silver aggregate were calculated[17] using single crystal elastic constants.[16]

The temperature dependence shown in Fig. 3 is similar to that observed earlier[8,12,13,33] for pure soft metals. The spall strength of these metals varies weakly with temperature but drops abruptly at the immediate vicinity of the melting point. The increase of the dynamic yield strength of these metals with temperature is usually attributed to the interaction of moving dislocations with the oncoming phonon flow.[34]

A. Decay of the elastic precursor wave and initial plastic strain rate

Figure 5 presents the results of measurements of apparent HEL values for silver samples of various thickness impacted at temperatures 296, 973, 1173, and 1233 K. For the waveforms obtained at 296 K it was impossible to identify the HEL value. In this case the stress $\sigma_{0.05}$ corresponding to the 0.05% offset of plastic strain γ_p ($\gamma_p = 0.0005$) was used instead. The values of $\sigma_{0.05}$ (some $\pm$ 10% uncertainty) have been estimated using the simple wave approximation.

The stress relaxation caused by the development of plastic deformation behind the precursor front results in the decay of the elastic precursor amplitude σ_{HEL} with propagation distance.[19,20] Experimental data in Fig. 5 are well described by the empirical relationships

$$\sigma_{\mathrm{HEL}} = S(h/h_0)^{-\alpha}, \tag{1}$$

where $h_0 = 1$ mm, and the exponent α varies from 0.506 at 973 K to 0.597 at 1233 K. In spite of the wider scatter, the data on the precursor decay at 1173 K yield the value $\alpha = 0.55$ with the Pearson correlation coefficient $p = 0.97$ only slightly lower than for two other temperatures, $p = 0.99$. Note that the values of α obtained with the silver samples are close to $\alpha = 0.57$ found for precursor decay in aluminum[21] over the propagation distances ranging from 10^{-3} mm to 10 mm. On the basis of Eq. (1), one can conclude that the abnormally high HEL values observed at elevated temperatures in the samples of sub-millimeter thickness should not be observed for the samples whose thickness exceeds 10–20 mm.

The elastic precursor decay is related to the plastic strain rate $\dot{\gamma}_p$ behind its front as[19]

$$\left.\frac{d\sigma}{dh}\right|_{\mathrm{HEL}} = -\frac{4}{3}\frac{G\dot{\gamma}_p}{c_l}, \tag{2}$$

where G is the material shear modulus and h is the propagation distance. The relationship (2) has been obtained in an acoustic approach with assumption that the sound speed c_l and the propagation speed of the elastic precursor front $U_E = c_l$ are constant. More detailed description[20] accounts for the dependences of these speeds on the stress and for the hydrodynamic decay due to the stress gradient behind the elastic shock wave. Such a correction, however, is not essential in the present case of the relatively low HEL values and

small stress gradients. It should be emphasized that the Eq. (2) (as well as more detailed similar relationships) follow immediately from an analysis of the wave dynamics in relaxing media. No additional assumptions about either mechanism or kinetics of plastic deformation or interaction between elastic and plastic waves are required. The precursor decay is controlled only by initial plastic strain rate behind its front and does not depend on further process of establishing the steady plastic shock wave.

After substituting the empirical dependence (1) into Eq. (2) we have

$$\dot{\gamma}_p = \frac{3}{4}\frac{S\alpha c_l (h/h_0)^{-(\alpha+1)}}{h_0 G}. \tag{3}$$

In this case the relationship between the maximum shear stress under uniaxial compression $\tau = \sigma_{\mathrm{HEL}} G/E'$[31] (where $E' = \rho_0 c_l^2$ is the longitudinal elastic modulus) and the plastic strain rate $\dot{\gamma}_p$ is

$$\dot{\gamma}_p = \frac{3}{4}\left(\frac{\tau E'}{SG}\right)^{(\alpha+1)/\alpha}\frac{S\alpha c_l}{h_0 G}. \tag{4}$$

Figure 6 presents the dependences $\dot{\gamma}_p = 1.45(\tau/44.4)^{2.98} \times 10^4\ \mathrm{s}^{-1}$, $\dot{\gamma}_p = 2.55(\tau/60.7)^{2.82} \times 10^4\ \mathrm{s}^{-1}$, and $\dot{\gamma}_p = 4.4(\tau/91.5)^{2.68} \times 10^4\ \mathrm{s}^{-1}$ of the initial plastic strain rate behind the precursor front on the shear stress at HEL (in MPa) for, respectively, 973, 1173, and 1233 K. A linear dependence of the plastic strain rate on the shear stress corresponding to a constant Newtonian viscosity η is shown in Fig. 6 for comparison.

It is apparent from Fig. 6 that both the yield strength and the plastic strain rate behind the precursor front at fixed propagation distance (open circles) increase with temperature. Approaching the melting temperature facilitates this growth;

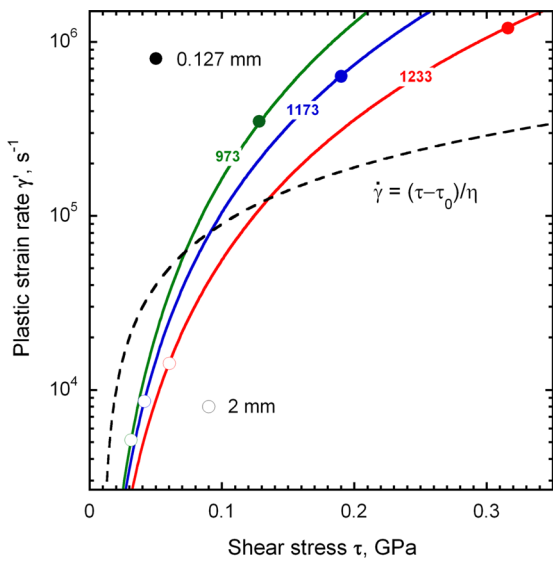

FIG. 6. (Color online) Initial plastic strain rates behind the elastic precursor front as function of the shear stress at different temperatures. The symbols correspond to the stresses and strain rates at the thickest (2 mm, open circles) and the thinnest (0.127 mm, filled circles) samples. The dependence $\dot{\gamma}_p = (\tau-\tau_0)/\eta$ corresponding to the constant Newtonian viscosity is shown by dashed line.

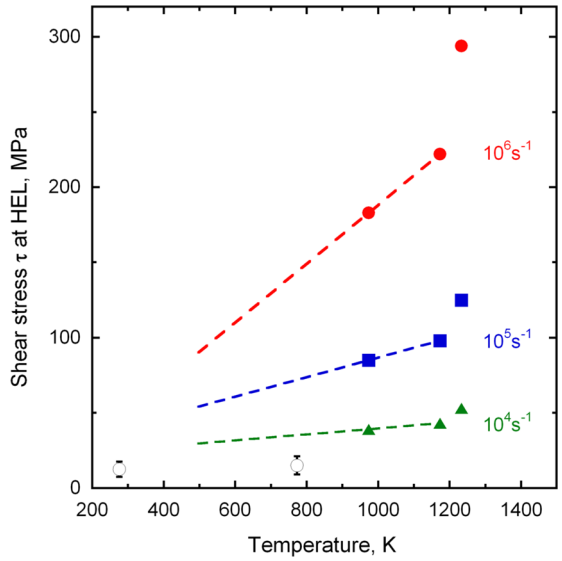

FIG. 7. (Color online) Variations of the shear stress at elastic precursor front with increasing temperature at three fixed strain rates (filled patterns). The shear stress values at 276 and 773 K (open circles) are shown for orientation. The latter values are approximate and are not associated with any certain strain rate. The dashed line corresponds to the linear dependence of the yield strength on temperature far off the vicinity of the melting temperature.

the temperature variations of the yield strength at the constant level of the plastic strain rate, Fig. 7, demonstrate a steep strengthening near melting. Similar abrupt increase of the dynamic yield strength near melting was observed in the experiments with tin.[13] Moreover, approaching the temperature of the solid-solid phase transformation ($\alpha \rightarrow \gamma$ transformation in iron,[10] $\alpha \rightarrow \beta$ transformation in titanium[35]) also results in a sharp increase of the dynamic yield strength in the close vicinity of the transformation. It appears that approaching the limit of lattice stability is accompanied by an enhancement of the lattice resistance to high-rate deformation. Below 1173 K, the data in Fig. 7 are compatible with a linear dependence of the flow stress on temperature expected in the case of dislocations drag caused by phonon friction.

B. High-rate deformation in plastic shock wave

An alternative source of information about the flow stress at high strain rates is the plastic shock wave.[25–27] The strain rate in the plastic shock wave is determined by the time derivative of the free surface velocity history. Even if the plastic shock wave is not perfectly steady, the uncertainty of such estimate of the plastic strain rate is limited.[27] Determining the flow stress on the basis of the plastic part of the recorded velocity history is more delicate problem. Two approximations are usually used in solving the problem. The simple wave approximation[36] implies a constant propagation velocity for each part of the unsteady wave. The steady wave approximation implies a permanent shape of the wave together with the permanence of the states both ahead and behind the plastic shock wave. As it is apparent from Fig. 3, the simple wave approximation cannot be used in the present case; the variation, with the propagation distance, of the time

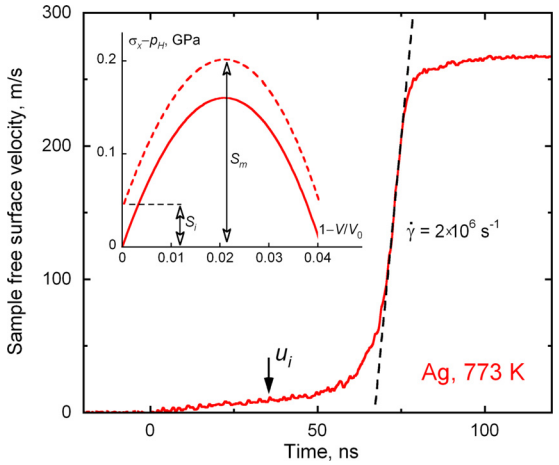

FIG. 8. (Color online) Schematics of estimating the maxima of the plastic strain rate and shear stress behind the plastic front.

intervals between the elastic and plastic waves imply inconstancy of the velocity of the plastic front.

Assuming that for 2 mm samples the flow is quite steady, we used the scheme shown in Fig. 8 for a rough estimating the maximum values of the shear stress and the plastic strain rate behind the plastic shock front. The total strain rate in the plastic shock wave $\dot{\varepsilon}_x$ was determined as the maximum time derivative of the free surface velocity divided by twice the velocity of the steady wave front: $\dot{\varepsilon}_x = \dot{u}_{fs}/2U_S$. (The recorded velocity histories are slightly distorted by multiple reverberations of the elastic waves between the sample free surface and the plastic shock front.[31] As a result, the actual, in-material, plastic wave is steeper than that recorded at the free sample surface and the strain rate estimates correspond to their bottom limit.)

The maximum shear strain rate at uniaxial compression, $\dot{\gamma} = \dot{\varepsilon}_x/2$, is the sum of elastic component, $\dot{\gamma}_e = \dot{\tau}/2G$, and plastic shear strain rate $\dot{\gamma}_p$. As a result we have

$$\dot{\gamma}_p = \frac{\dot{\varepsilon}_x}{2} - \frac{\dot{\tau}}{2G}. \tag{6}$$

In the steady plane shock wave, the loading path follows the Rayleigh line, the straight line connecting the states ahead of

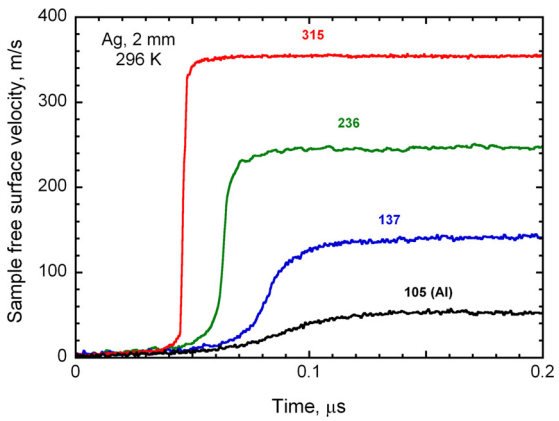

FIG. 9. (Color online) The free surface velocity history of the 2 mm silver samples impacted by copper flyer plates at impact velocities varied from 105 m/s (Al impactor) to 315 m/s.

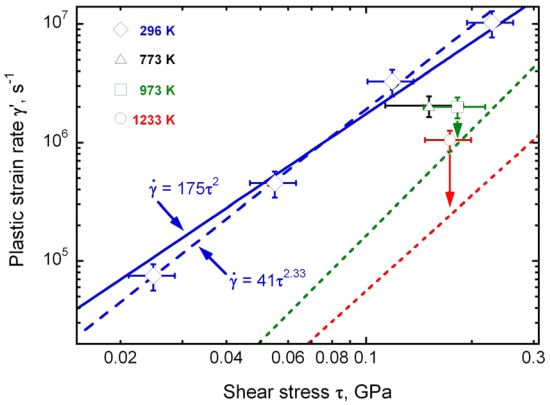

FIG. 10. (Color online) Plastic strain rate as a function of shear stress in plastic shock wave at different temperatures (open symbols). The solid line corresponds to the approximation $\dot{\gamma}_p = K_2(\tau/\tau_0)^2$ of the room-temperature data, while the dashed line represents the best fit $\dot{\gamma}_p = K_{2.3}(\tau/\tau_0)^{2.3}$ for these data. The dot-dashed lines are the $\dot{\gamma}(\tau)$ dependence of the initial plastic strain rate on the shear stress, shown in Fig. 6.

the wave and behind it. The deviatoric stress $S_x = \sigma_x - p$ can be determined as the difference between the stress σ_x on the Rayleigh line and the pressure p on the material Hugoniot at the same total strain.[26,37] In this case, the shear stress $\tau = (3/4)S_x$ has to pass through a maximum (see insert in Fig. 8). At the maximum $\dot{\tau} = 0$ and $\dot{\gamma}_p = \dot{\varepsilon}_x/2$. The total shear stress at the maximum was estimated as the shear stress corresponding to the maximum stress deviator plus the shear stress value corresponding to the stress deviator S_i (Fig. 8) ahead of shock wave. The value of S_i was calculated using expression $S_i = \rho_0 c_l(1 - c_b^2/c_l^2)u_i/2$, where u_i is the free surface velocity at the midpoint between the leading part of the elastic precursor and the plastic wave (Fig. 8).

At room temperature the silver samples of 2 mm thickness were tested at different peak stresses. The free surface velocity history recorded in these tests is shown in Fig. 9. The plastic strain rates and the maximum shear stresses corresponding to the velocity histories were estimated within the steady wave approximation, as described above. The $\dot{\gamma}_{p\max}(\tau_{\max})$ data obtained after the room temperature experiments are shown in Fig. 10 together with four $\dot{\gamma}_{p\max}(\tau_{\max})$ points estimated on the basis of the velocity histories obtained with the 2 mm silver samples preheated up to 733, 973, and 1233 K. As apparent from Fig. 10, the room temperature data are in a reasonable agreement with the dependence of the strain rate on the squared shear stress, $\dot{\gamma}_p = K_2(\tau/\tau_0)^2$, which has been established for several metals.[26,27] In the present case $K_2 = 175$ s^{-1} and $\tau_0 = 1$ MPa. The best fit of the room temperature data suggests, however, a slightly different expression $\dot{\gamma}_p = K_{2.3}(\tau/\tau_0)^{2.3}$ with $K_{2.3} = 41$ s^{-1}. The stress error bars in Fig. 10 correspond to the uncertainties in the stress states behind the plastic shock wave; the strain hardening should result in a deviatoric stress greater than S_i, whereas the multiplication of mobile dislocations may provide relaxation of the deviatoric stress toward values lower than S_i. The rise time of plastic shock wave and the characteristic viscosity $\eta = \tau/\dot{\gamma}_p$ in plastic shock wave grow with temperature. This finding can be derived from Fig. 10 as a decrease with temperature of the plastic strain

rate $\dot{\gamma}$ at fixed shear stress τ. Comparing the strain rates at the mid-height of the plastic front with the initial plastic strain rates behind the precursor front (Fig. 10) allows one to conclude that at the same level of the shear stress the plastic deformation at the shock wave is much faster. Such enhancement of the strain rate may be considered as an evidence of an intense multiplication of mobile dislocations.

IV. CONCLUSION

The evolution of the elastic-plastic shock waves in 99.9 % purity silver have been recorded with VISAR for sample thickness varied from 0.127 to 2.0 mm at initial sample temperature varied from 300 to 1233 K. The data confirm the anomalous thermal strengthening of fcc metals at high strain rates. The free surface velocity histories at room temperature and 773 K do not show any distinct step-like feature at the leading edge of the elastic precursor wave. Starting from 973 K, the waveforms clearly exhibit finite HEL amplitude whose value grows with temperature and decreases with t sample thickness. The amplitude of the elastic precursor wave at 973, 1173, and 1233 K temperatures is approximately inversely proportional to the square root of the propagation distance. The latter corresponds to a cubic dependence of initial plastic strain rate on the shear stress at HEL. With exception of the close vicinity of the silver melting point, the temperature effect on the flow stress at fixed strain rate is compatible with the strength mechanism based on dislocation deceleration by the oncoming phonon flow. Approaching the melting point is accompanied by a sharp increase of the flow stress and implies the involvement of an additional mechanism(s) of the dislocation drag. The analysis of the rise times of the plastic shock waves confirms the approximately linear relation between the squared shear stress and the plastic strain rate. Given the same level of the shear stress, the latter was found to be much higher than that at the top of the elastic precursor wave.

Most of the atomistic simulations of the motion of dislocations show approximately linear dependences of the dislocation velocities on the shear stress at moderate stress level. When the dislocation velocity approaches the value of the shear speed of sound in the material, its dependence on stress becomes much weaker. The presently observed stronger than linear dependences of the plastic strain rates on temperature may be associated with the activation of additional slip and twin systems that involve less favorably oriented grains into the plastic deformation process. It may also imply a growing contribution of nucleation and multiplication of dislocations in the plastic straining. Although the presently obtained experimental data do not allow deriving more definite conclusions regarding the particular contribution of each of these processes, they can be used for verification of hypothetical mechanisms of high-rate plastic deformation. In this regard, similar sets of experiments with single crystals would be useful.

ACKNOWLEDGMENTS

Financial support from Israeli Science Foundation via research Grant No. 56/09 (85300221), from Israeli Planning and Budget Committee for High Education via research Grant No. 84647601 and from Russian Foundation for Basic Research via the Grant No. 11-02-01141-a is gratefully acknowledged.

[1]A. Kumar and R. G. Kumble, J. Appl. Phys. **40**(9), 3475(1969).
[2]M. A. Meyers, D. J. Benson, O. Vohringer, B. K. Kad, Q. Xue, and H.-H. Fu, Mater. Sci. Eng. A **322**, 194 (2002).
[3]T. Hatano, Phys. Rev. Lett. **93**, 085501 (2004).
[4]V. A. Al'shitz and V. L. Indenbom, Sov. Phys. Usp. **18**(1), 1 (1975).
[5]A. Y. Kuksin, G. E. Norman, V. V. Stegailov, and A. V. Yanilkin, J. Eng. Thermophys. **18**(3), 197 (2009).
[6]G. I. Kanel, S. V. Razorenov, K. Baumung, and J. Singer, J. Appl. Phys. **90**(1), 136 (2001).
[7]G. I. Kanel, S. V. Razorenov, E. B. Zaretsky, B. Herrman, and L. Meyer, Phys. Solid State **45**(4), 656 (2003).
[8]G. I. Kanel, S. V. Razorenov, and V. E. Fortov, J. Phys.: Condens. Matter **16**(14), S1007 (2004).
[9]G. V. Garkushin, G. I. Kanel', and S. V. Razorenov, Phys. Solid State **52**(11), 2369 (2010).
[10]E. B. Zaretsky, J. Appl. Phys. **106**, 023510 (2009).
[11]V. Favorsky and E. B. Zaretsky, J. Appl. Phys. **108**, 073528 (2010).
[12]E. B. Zaretsky, J. Appl. Phys. **108**, 083525 (2010).
[13]E. B. Zaretsky and G. I. Kanel, EDP Sciences **1**, 27 (2009).
[14]S.-N. Luo, Q. An, T. C. Germann, and L.-B. Han, J. Appl. Phys. **106**, 013502 (2009).
[15]A. W. Ruff, Jr. and L. K. Ives, Acta Metall. **15**, 189 (1967).
[16]A. Wolfenden and M. R. Harmouche, J. Mater. Sci. **28**, 1015 (1993).
[17]R. Hill, Proc. Phys. Soc. A **65**, 349 (1952).
[18]R. Iya, *CRC Handbook of Chemistry and Physics*, 91st edition, internet version, edited by D. R. Lide (CRC Press/Taylor and Francis, Boca Raton, FL, 2011).
[19]G. E. Duvall, Propagation of plane shock waves in a stress-relaxing medium, in *Stress Waves in Anelastic Solids*, edited by H. Kolsky and W. Prager (Springer-Verlag, Berlin, 1964) pp. 20–32.
[20]J. R. Asay, G. R. Fowles, and Y. Gupta, J. Appl. Phys. **43**, 744 (1972).
[21]S. I. Ashitkov, M. B. Agranat, G. I. Kanel', P. S. Komarov, and V. E. Fortov, JETP Lett., **92**(8), 516 (2010).
[22]Y. M. Gupta, J. M. Winey, P. B. Trivedi, B. M. LaLone, R. F. Smith, J. H. Eggert, and G. W. Collins. J. Appl. Phys. **105**, 036107 (2009).
[23]J. M. Winey, B. M. LaLone, P. B. Trivedi, and Y. M. Gupta, J. Appl. Phys. **106**, 073508 (2009).
[24]J. N. Johnson and L. M. Barker, J. Appl. Phys. **40**, 4321 (1969).
[25]L. C. Chhabildas and J. R. Asay, J. Appl. Phys. **50**(4), 2749 (1979).
[26]J. W. Swegle and D. E. Grady, J. Appl. Phys. **58**, 692 (1985).
[27]D. E. Grady, J. Appl. Phys. **107**, 013506 (2010).
[28]L. M. Barker and R. E. Hollenbach, J. Appl. Phys. **43**, 4669 (1972).
[29]T. Mashimo, Y. Hanaoka, and K. Nagayama, J. Appl. Phys. **63**, 327 (1988).
[30]W. Arnold, in *Shock Compression of Condensed Matter* 1991, edited by S. C. Schmidt, R. D. Dick, J. W. Forbes, and D. G. Tasker (Elsevier, New York, 1992), pp. 539–542.
[31]G. I. Kanel, S. V. Razorenov, and V. E. Fortov, *Shock Wave Phenomena and the Properties of Condensed Matter* (Springer, New-York, 2004), p. 33.
[32]T. Antoun, L. Seaman, D. Curran, G. I. Kanel, S. V. Razorenov, and A. V. Utkin, *Spall Fracture* (Springer, New-York, 2002), pp. 90, 99.
[33]G. I. Kanel, S. V. Razorenov, A. A. Bogatch, A. V. Utkin, V. E. Fortov, and D. E. Grady, J. Appl. Phys. **79**, 8310 (1996).
[34]A. D. Brailsford, J. Appl. Phys. **43**, 1380 (1972).
[35]E. B. Zaretsky, J. Appl. Phys. **104**, 123505 (2008).
[36]R. Fowles and R. F. Williams, J. Appl. Phys. **41**, 360 (1970).
[37]G. R. Cowan. Trans. Metal. Soc. AIME **233**(6), 112 (1965).